ISSN 1087-6596, Glass Physics and Chemistry, 2023, Vol. 49, No. 1, pp. 41–49. © Pleiades Publishing, Ltd., 2023.
Russian Text © The Author(s), 2023, published in Fizika i Khimiya Stekla.

# Vapor Formation and the Thermodynamic Properties of the $SrO–Al_2O_3–SiO_2$ System

**N. G. Tyurnina[a], S. I. Lopatin[a, *], S. M. Shugurov[a, b], Z. G. Tyurnina[a], I. G. Polyakova[a], and E. A. Balabanova [a]**

[a] *Grebenshchikov Institute of Silicate Chemistry, Russian Academy of Sciences, St. Petersburg, 199034 Russia*
[b] *St. Petersburg State University, St. Petersburg, 199034 Russia*
**e-mail: sergeylopatin2009@yandex.ru*

Received August 18, 2022; revised September 16, 2022; accepted October 27, 2022

**Abstract**—Vaporization and thermodynamic properties of the $SrO–Al_2O_3–SiO_2$ system are studied by high-temperature differential mass spectrometry in the concentration range from 90 to 10 mol % of SrO and the molar ratio of $x(Al_2O_3)/x(SiO_2) = 1.5$. The samples are evaporated from Knudsen effusion chambers made of tungsten. The partial pressures of the molecular forms of the vapor, the activities of the condensed phase components, the Gibbs energies, and the excess Gibbs energies are determined. It is established that the studied system is characterized by a slight negative deviation from the ideal behavior. For mullite ($Al_6Si_2O_{13}$) the value of the standard enthalpy of formation is determined. The melting points of the synthesized samples are established by high-temperature microscopy.

**Keywords:** in high-temperature mass spectrometry, vaporization, oxides of strontium, aluminum and silicon, activity, Gibbs energy, melting points

**DOI:** 10.1134/S1087659622600909

## INTRODUCTION

The development of aviation and space technology requires the development of new materials with specific physical and chemical properties. When designing aircraft, one should first of all take into account the fact that parts of aircraft and spacecraft will be exposed to extremely high temperatures during operation. The efficiency of using various aerospace systems is largely determined by the characteristics of the radio engineering devices placed onboard [1]. To protect these devices from external influences, various radiotransparent materials with sufficiently high thermal stability are used. Glass ceramics based on aluminosilicate systems are used as such materials. In recent years, researchers have paid increased attention to materials based on $SrO–Al_2O_3–SiO_2$ (SAS) and $BaO–Al_2O_3–SiO_2$ (BAS) systems, which have high melting points, thermal stability, and good strength properties, which make them promising for the fabrication of radiotransparent materials [2–4]. Composite materials based on SAS and BAS have high resistance to thermal shock, high chemical resistance, and stable dielectric properties, which make these materials suitable for manufacturing high-temperature antenna radomes and radio-transparent windows of high-speed aircraft with an operating temperature of at least 2300 K.

During the operation of radiotransparent ceramics at high temperatures, processes of selective evaporation of more volatile components may occur, leading to an irreversible change in specific properties. In relation to this, one of the main tasks is to experimentally study the vaporization and thermodynamic properties of glass-ceramic radio-transparent materials in order to identify compositions with the maximum thermal stability.

The most volatile components in the $SrO–Al_2O_3–SiO_2$ system are strontium oxide and silicon dioxide [5], which begin to transform into vapor at temperatures on the order of 1900 to 2000 K. The formation of solid solutions and thermally stable compounds in $SrO–Al_2O_3$ [6–8], $SrO–SiO_2$ [9–11], and $Al_2O_3–SiO_2$ [12–27] binary systems, as well as in the $SrO–Al_2O_3–SiO_2$ ternary system [28–30], reduces the activity of the condensed phase components and increases the vaporization temperature. Figure 1 shows a diagram of the triangles of coexisting phases in the subsolidus region and Fig. 2 contains the melting diagram of the $SrO–Al_2O_3–SiO_2$ system.

## EXPERIMENTAL

The vaporization processes and thermodynamic properties of the $SrO–Al_2O_3–SiO_2$ were studied by high-temperature mass spectrometry on an MS-1301

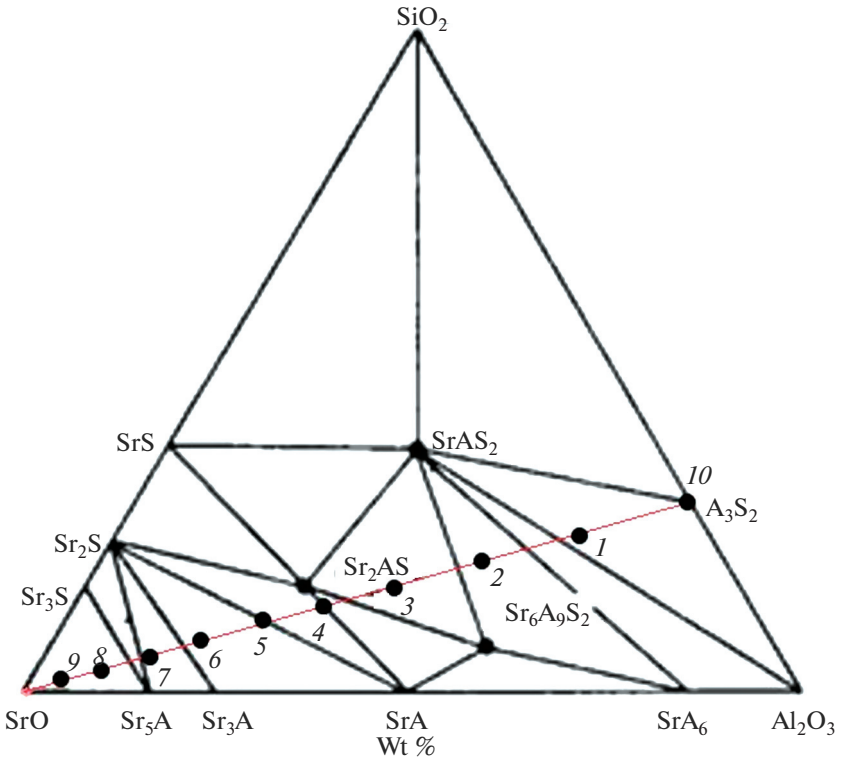


**Fig. 1.** Triangle diagram of coexisting phases of the $SrO–Al_2O_3–SiO_2$ system in the subsolidus region at a temperature of 1623 K [31].

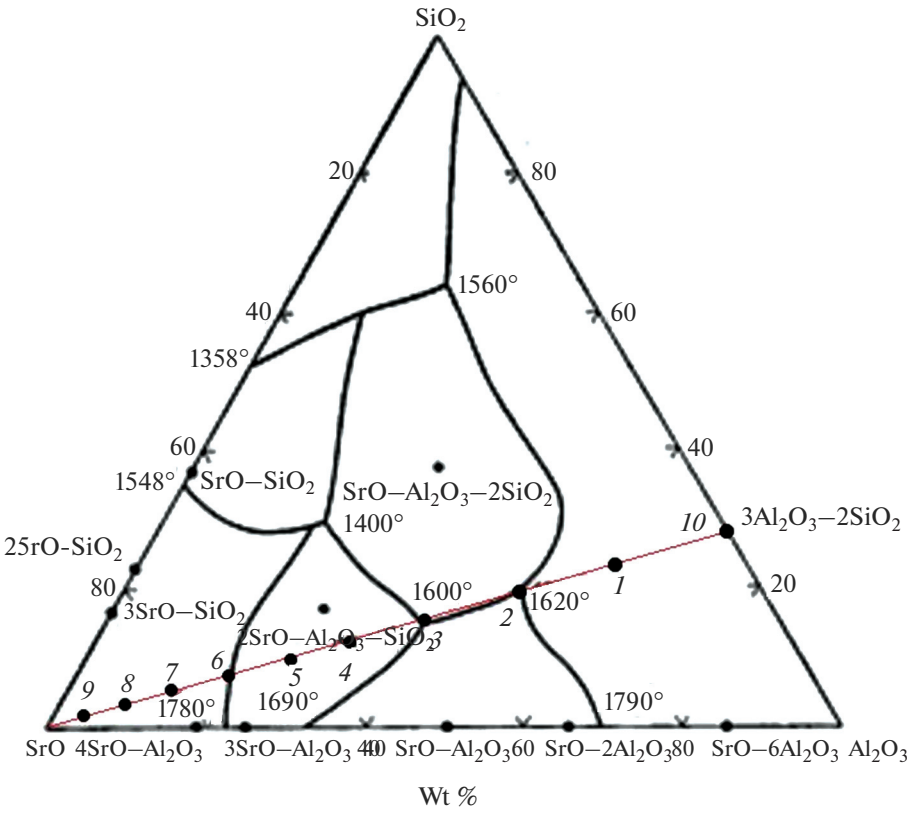


**Fig. 2.** Melting diagram of the $SrO–Al_2O_3–SiO_2$ system [32].

mass spectrometer (SKB of Analytical Instrumentation of the Academy of Sciences of the USSR, Leningrad) at an energy of ionizing electrons of 30 eV. The studied samples were evaporated from a double single-temperature Knudsen chamber made of tungsten. A sample was loaded into one of the cells of the chamber, and oxides of strontium or silicon alternately were loaded into the other, comparative cell. The chamber was heated by electron bombardment, and the temperature was measured with an EOP-66 optical pyrometer. The equipment was preliminarily calibrated against the vapor pressure of $CaF_2$ [33].

In this study, in the $SrO–Al_2O_3–SiO_2$ system, ten samples were synthesized by solid-phase synthesis (SPS), whose compositions lie on the secant phase diagram of the $SrO–Al_2O_3–SiO_2$ system (Figs. 1 and 2) [31, 32]. The chemical composition of the samples (by synthesis) is indicated in Figs. 1 and 2 by points and is presented in Table 1. The point numbers in Figs. 1 and 2 correspond to the sample numbers in Table 1. In the synthesis, $SrCO_3$, $Al_2O_3$, and crystalline $SiO_2$ were used as the initial reagents. All reagents were of analytical grade. For homogenization, the sample was ground in a Retsch PM 100 planetary ball mill for 2 h and pressed into tablets 1 cm in diameter in a hydraulic press at a pressure of 4 tons. The obtained tablets were calcined in a Naberthem Top 16/R muffle furnace in corundum crucibles at 1523 K for 12 h. The samples were cooled together with the furnace. Next, the samples were crushed in an agate mortar and their X-ray phase analysis was carried out to control the achievement of equilibrium by the samples. If the equilibrium phase composition was not achieved, repeated calcination was carried out under the same conditions.

The degree of interaction of the initial reagents in the synthesized samples was controlled by X-ray phase analysis (XPA) on a DRON-3M diffractometer using Cu$K_\alpha$-radiation. The measurements were carried out in a continuous mode at the $2\Theta$ diffraction angles in the range from 10° to 70° at a scanning rate of 2°/min. The crystalline phases were identified using the PDF-2 powder diffractometry database.

The X-ray diffraction patterns of the synthesized ceramic samples in the $SrO–Al_2O_3–SiO_2$ system with the identification of crystalline phases are presented in Figs. 3 and 4.

Table 2 shows the phase composition of the samples in the $SrO–Al_2O_3–SiO_2$ system after isothermal holding for 12 h and 24 h at an SPS temperature of 1523 K, and also the melting points of the obtained samples measured on a high-temperature microscope (HTM), whose design was developed at the Institute of Chemical Chemistry of the Russian Academy of Sciences [34]. The temperature determination error was ±20 K.

The XPA data (Figs. 3, 4, Table 2) show the formation in sample nos. 1–8 of at least two clearly fixed phases that satisfactorily correspond to the triangulation presented in Fig. 1. Sample no. 8, in which the crystalline compound $Sr_4Al_2O_7$, absent in the $SrO–Al_2O_3–SiO_2$ phase diagram, according to [31], but present in the PDF-2 database and on the phase diagram of the ternary system in [35], is an exception. The third phase cannot be determined precisely because of its low content in the samples and numerous overlapping peaks.

**Table 1.** Chemical composition of samples (by synthesis)

| N | The content of oxides, mol % | | |
|---|---|---|---|
| | SrO | $Al_2O_3$ | $SiO_2$ |
| 1 | 10 | 54 | 36 |
| 2 | 20 | 48 | 32 |
| 3 | 30 | 42 | 28 |
| 4 | 40 | 36 | 24 |
| 5 | 50 | 30 | 20 |
| 6 | 60 | 24 | 16 |
| 7 | 70 | 18 | 12 |
| 8 | 80 | 12 | 8 |
| 9 | 90 | 6 | 4 |
| 10 | 0 | 60 | 40 |

Comparison of the phase composition of the samples obtained during isothermal exposure for 12 and 24 h at a temperature of 1523 K shows that the phase equilibrium is achieved either in 12 h or not at all, as is the case in sample nos. 9 and 10. Sample no. 10 has a stoichiometric composition corresponding to mullite ($3Al_2O_32SiO_2$); however, even after daily heat treatment, there are no signs of the formation of mullite in it. The sample remains the same mixture of quartz and corundum as its original charge. Sample no. 9, containing in the original composition 90 mol % SrO, upon subsequent storage in air, interacts with moisture, forming hydroxide $Sr(OH)_2$, which is recorded in sample no. 9 during X-ray photography. In addition to strontium hydroxide, this sample also contains quartz. The X-ray diffraction patterns of sample no. 9, kept for 12 and 24 h at a temperature of 1523 K, are almost identical; no interaction between the components is detected. In sample no. 8, after 12 hours of exposure at a temperature of 1523 K, together with silicate and strontium aluminate (Table 2), its hydroxide $Sr(OH)_2$ is also recorded, which indicates the presence of residual, unreacted SrO in the hot sample. After increasing the isothermal exposure to 24 h, strontium oxide completely reacts with the formation of aluminate and silicate, and traces of strontium hydroxide are no longer detected on the X-ray diffraction pattern of the cold sample no. 8 (Fig. 4). Thus, we observe the reduced reactivity of oxides not only in sample no. 10, which

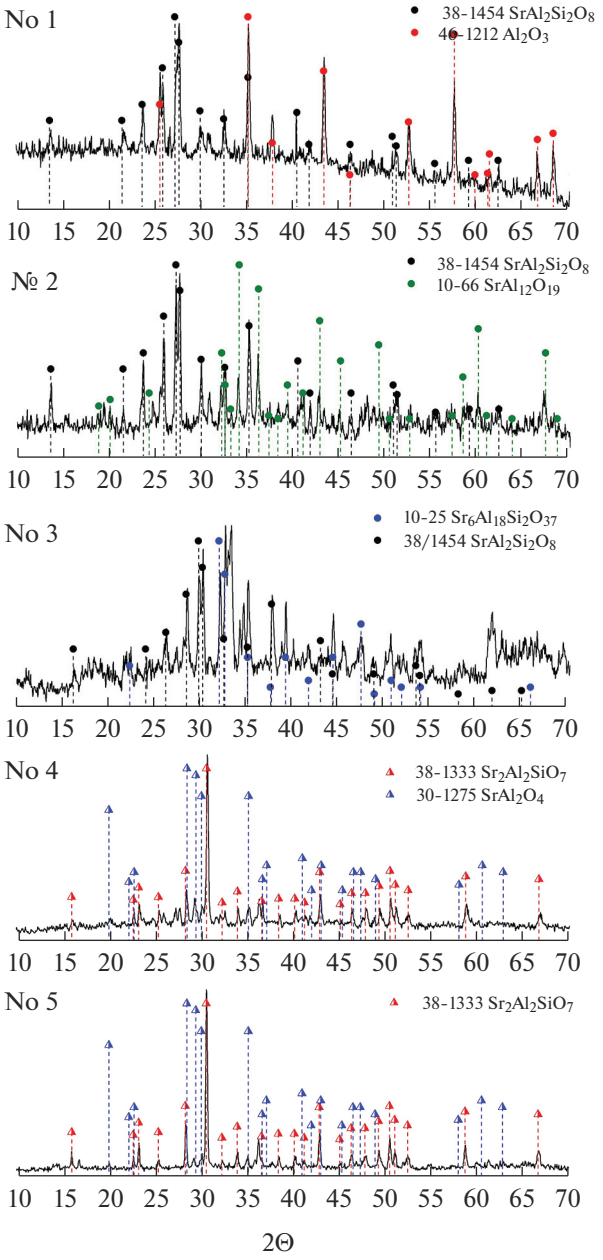


**Fig. 3.** X-ray diffraction patterns of samples annealed at 1523 K for 12 h (nos. 1, 2) and 24 h (nos. 3–5).

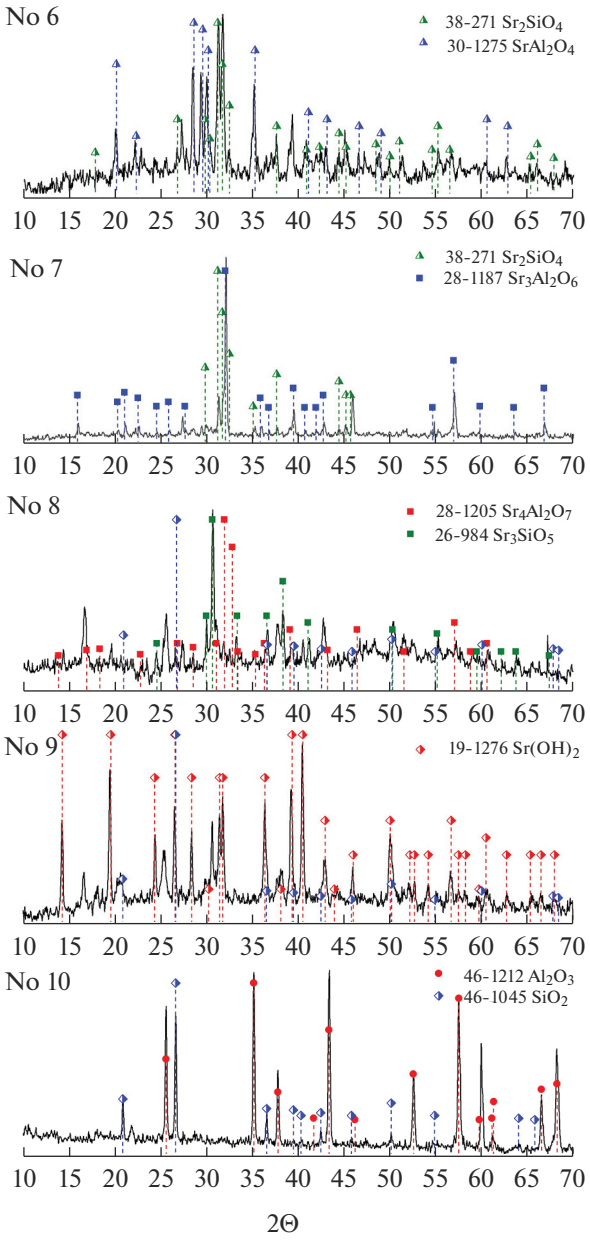


**Fig. 4.** Diffractograms of sample nos. 6, 8–10, annealed at 1523 K for 24 h, and no. 7 –, for12 hours

does not contain SrO, but also in sample no. 9, which contains a significant excess of it.

In the mass spectra of vapor over the studied samples in the temperature range 1950–2010 K, peaks of $Sr^+$ and $SiO^+$ ions were recorded, whose intensity ratio at a fixed temperature depended on the initial composition of the sample. During isothermal holding, the intensity of ion currents of $Sr^+$ and $SiO^+$ gradually decreased. In the mass spectra of vapor over sample nos. 1–3 and 10, ions $WO_2^+$ and $WO_2^+$, formed during the ionization of the corresponding molecules, which are the result of the interaction of samples with the material of the effusion chamber, were recorded. To search for molecular precursors of $Sr^+$ and $SiO^+$ ions, the energies at which they occurred were measured by the vanishing ion current method [36]. The obtained values 5.8 ± 0.3 and 11.5 ± 0.3 eV, respectively, coincide with the ionization energies of atomic strontium and silicon monoxide [37]. As the temperature increased to 2250 K, $Al^+$, $AlO^+$, and $Al_2O^+$ ions appeared in the mass spectra of the vapor at energies of their occurrence of 6.1, 9.6, and 7.9 eV, respectively. An analysis of the mass spectra of the vapor over the

**Table 2.** Phase composition of samples in the $SrO–Al_2O_3–SiO_2$ system after exposure at a temperature of 1523 K for 12 and 24 h and their melting points ($T_{pl}$) according to the HTM

| N | Mol % | | | Phase composition | | $T_{melt}$, K |
|---|---|---|---|---|---|---|
| | SrO | $Al_2O_3$ | $SiO_2$ | 1523 K 12 h | 1523 K 24 h | |
| 1 | 10 | 54 | 36 | $Al_2O_3$<br>$SrAl_2Si_2O_8$ | – | 1848 |
| 2 | 20 | 48 | 32 | $SrAl_2Si_2O_8$<br>$SrAl_{12}O_{19}$ | – | 1858 |
| 3 | 30 | 42 | 28 | $Sr_6Al_{18}Si_2O_{37}$<br>$Sr_2Al_2SiO_7$ | $Sr_6Al_{18}Si_2O_{37}$<br>$SrAl_2Si_2O_8$ | 1833 |
| 4 | 40 | 36 | 24 | $Sr_2Al_2SiO_7$<br>$SrAl_2O_4$ | $Sr_2Al_2SiO_7$<br>$SrAl_2O_4$ | 1815 |
| 5 | 50 | 30 | 20 | $Sr_2Al_2SiO_7$<br>$SrAl_2O_4$ | $Sr_2Al_2SiO_7$<br>$SrAl_2O_4$ | 1843 |
| 6 | 60 | 24 | 16 | $SrAl_2O_4$<br>$Sr_2SiO_4$ | $SrAl_2O_4$<br>$Sr_2SiO_4$ | 1929 |
| 7 | 70 | 18 | 12 | $Sr_3Al_2O_6$<br>$Sr_2SiO_4$ | – | 1913 |
| 8 | 80 | 12 | 8 | $Sr_3SiO_5$<br>$Sr_4Al_2O_7$<br>$Sr(OH)_2$ | $Sr_3SiO_5$<br>$Sr_4Al_2O_7$ | 1898 |
| 9 | 90 | 6 | 4 | $Sr(OH)_2$<br>$SiO_2$ | $Sr(OH)_2$<br>$SiO_2$ | – |
| 10 | 0 | 60 | 40 | $Al_2O_3$<br>$SiO_2$ | $Al_2O_3$<br>$SiO_2$ | – |

studied samples and the energies of the appearance of ions in the mass spectra of the vapor indicate that, in the temperature range of 1950 to 2010 K, SiO, atomic strontium, and oxygen pass into the vapor according to equations of reactions (1) and (2).

$$SrO(\text{тв., ж}) = Sr(\text{г}) + O(\text{г}), \quad (1)$$

$$SiO_2(\text{тв., ж}) = SiO(\text{г}) + O(\text{г}). \quad (2)$$

In this case, aluminium accumulates in the condensed phase, which passes into vapor at a higher temperature according to Eqs. (3–5).

$$Al_2O_3(s, l) = 2Al(g) + 3O(g), \quad (3)$$

$$Al_2O_3(s, l) = 2AlO(g) + O(g), \quad (4)$$

$$Al_2O_3(s, l) = Al_2O(g) + 2O(g). \quad (5)$$

The partial pressures of atomic strontium and SiO were determined by comparing ion currents [36] using Eqs. (6) and (7), respectively.

$$p(Sr) = p_0(Sr)\frac{I\left(Sr^+\right)}{I_0\left(Sr^+\right)}, \quad (6)$$

$$p(SiO) = p_0(SiO)\frac{I\left(SiO^+\right)}{I_0\left(SiO^+\right)}. \quad (7)$$

Here $p$ and $p_0$ are partial vapor pressures above the sample and pressure standard, and $I$ and $I_0$ are the intensities of ion currents in the mass spectra of the vapor above the sample and the standard. Quantities $p_0$ were calculated by Eqs. (8) [8] and (9) [27], respectively.

$$\lg p(Sr, Pa) = \frac{-21839 \pm 547}{T} + (11.35 \pm 0.30), \quad (8)$$

$$\lg p(SiO, Pa) = \frac{-24676 \pm 552}{T} + (13.07 \pm 0.01). \quad (9)$$

The partial pressure of oxygen was not experimentally measured for a number of reasons. In particular, molecular beams of atomic and molecular oxygen repeatedly fly through the ionization region without condensing on the cold parts of the mass spectrometer. This significantly distorts the quantitative characteristics. In addition, oxygen is present in the residual gases of the mass spectrometer. Oxygen escaping from the Knudsen chamber is not blocked by the mass spec-

**Table 3.** Partial pressures of molecular forms of vapor over the studied samples of the $SrO–Al_2O_3–SiO_2$ system, values of the activities of the components of the condensed phase, and the Gibbs energies and excess Gibbs energies at a temperature of 2000 K

| Sample no. | Sample composition, mol % | | | $p_i$, Pa | | | $a_i$ | | | $-\Delta G(T)$, kJ | $-\Delta G^E(T)$, kJ |
|---|---|---|---|---|---|---|---|---|---|---|---|
| | SrO | $Al_2O_3$ | $SiO_2$ | Sr | SiO | O | SrO | $Al_2O_3$ | $SiO_2$ | | |
| 10 | 0 | 60 | 40 | – | 3.45 | 2.07 | 0 | 0.50 | 0.41 | 12.9 | 1.7 |
| 1 | 10 | 54 | 36 | $4.7 \times 10^{-3}$ | 2.96 | 1.77 | $3.0 \times 10^{-6}$ | 0.25 | 0.30 | 20.3 | 12.6 |
| 2 | 20 | 48 | 32 | $7.9 \times 10^{-3}$ | 2.16 | 1.29 | $8.6 \times 10^{-6}$ | 0.13 | 0.16 | 32.3 | 23.6 |
| 3 | 30 | 42 | 28 | $1.5 \times 10^{-2}$ | 1.91 | 1.14 | $3.3 \times 10^{-5}$ | $2.2 \times 10^{-2}$ | 0.125 | 43.9 | 34.9 |
| 4 | 40 | 36 | 24 | $6.1 \times 10^{-2}$ | 1.40 | 0.84 | $5.1 \times 10^{-4}$ | $3.4 \times 10^{-3}$ | $6.7 \times 10^{-2}$ | 47.6 | 38.7 |
| 5 | 50 | 30 | 20 | $9.3 \times 10^{-2}$ | 0.64 | 0.43 | $1.2 \times 10^{-3}$ | $1.8 \times 10^{-4}$ | $1.4 \times 10^{-2}$ | 56.5 | 48.0 |
| 6 | 60 | 24 | 16 | 0.12 | 0.50 | 0.31 | $2.0 \times 10^{-3}$ | $3.6 \times 10^{-6}$ | $8.7 \times 10^{-3}$ | 62.3 | 54.5 |
| 7 | 70 | 18 | 12 | 0.93 | 0.19 | 0.52 | 0.12 | $2 \times 10^{-10}$ | $1.3 \times 10^{-3}$ | 65.4 | 58.9 |
| 8 | 80 | 12 | 8 | 1.96 | – | 0.84 | 0.53 | – | – | – | – |
| 9 | 90 | 6 | 4 | 2.69 | – | 1.15 | 1.00 | – | – | – | – |

trometer damper, which separates the useful signal from the background one. As a result, the partial pressure of atomic oxygen was calculated using Eq. (10) [38].

$$p(\mathrm{O}) = p(\mathrm{Sr})\sqrt{\frac{M(\mathrm{O})}{M(\mathrm{Sr})}} + p(\mathrm{SiO})\sqrt{\frac{M(\mathrm{O})}{M(\mathrm{SiO})}}, \quad (10)$$

where $M$ is the molecular weight of the corresponding particle. The use of a double single-temperature Knudsen chamber made it possible to determine the activities of SrO and $SiO_2$ in the condensed phase according to Eqs. (11) and (12).

$$a(\mathrm{SrO}) = \frac{p(\mathrm{SrO})}{p_0(\mathrm{SrO})} = \frac{p(\mathrm{Sr})\,p(\mathrm{O})}{p_0(\mathrm{Sr})\,p_0(\mathrm{O})} = \frac{p^2(\mathrm{Sr})}{p_0^2(\mathrm{Sr})}, \quad (11)$$

$$a(\mathrm{O_2}) = \frac{p(\mathrm{SiO_2})}{p_0(\mathrm{SiO_2})} = \frac{p(\mathrm{SiO})\,p(\mathrm{O})}{p_0(\mathrm{SiO})\,p_0(\mathrm{O})} = \frac{p^2(\mathrm{SiO})}{p_0^2(\mathrm{SiO})}. \quad (12)$$

At a temperature of 2000 K, sample nos. 1–8, according to the phase diagram of the $SrO–Al_2O_3–SiO_2$ system [28, 39] belong to the region of a homogeneous melt. This made it possible to determine the activity of aluminum oxide using the Gibbs–Duhem equation, presented for this system in differential (13) and integral (14) forms. Integration was performed by a graphical method with extrapolation to infinite dilution [40].

$$x(\mathrm{SrO})\,d\ln a(\mathrm{SrO}) + x(\mathrm{Al_2O_3})\,d\ln a(\mathrm{Al_2O_3}) + x(\mathrm{SiO_2})\,d\ln a(\mathrm{SiO_2}) = 0, \quad (13)$$

$$\ln a(\mathrm{Al_2O_3}) = -\int_{\ln a^0(\mathrm{Al_2O_3})}^{\ln a(\mathrm{Al_2O_3})} \frac{x(\mathrm{SrO})}{x(\mathrm{Al_2O_3})}\,d\ln a(\mathrm{SrO}) - \int_{\ln a^0(\mathrm{Al_2O_3})}^{\ln a(\mathrm{Al_2O_3})} \frac{x(\mathrm{SiO_2})}{x(\mathrm{Al_2O_3})}\,d\ln a(\mathrm{SiO_2}). \quad (14)$$

The values of the activities of all track components of the condensed phase obtained for sample nos. 1–7 made it possible to determine the values of the Gibbs energies and excess Gibbs energies using Eqs. (15) and (16), respectively.

$$G = \sum x_i \ln a_i, \quad (15)$$

$$G^E = \sum x_i \ln \gamma_i. \quad (16)$$

Here $x_i$ is the mole fraction of the $i$th component of the melt, $a_i$ is the value of the activity of the $i$th component, and $\gamma_i$ is the activity coefficient of the $i$th component. The data obtained are presented in Table 3.

## RESULTS AND DISCUSSION

According to the data presented in Table 2, the phase composition of the samples is practically independent of the duration of isothermal exposure at a temperature of 1523 K. The only case of detecting a difference in the phase composition of the samples after 12 and 24 h of exposure at a temperature of 1523 K is related to sample no. 3 (Table 2). After 12 h of heat treatment, a mixture of two phases of $Sr_6Al_{18}Si_2O_{37}$ + $Sr_2Al_2SiO_7$, and after 24 h a mixture of $Sr_6Al_{18}Si_2O_{37}$ + $SrAl_2Si_2O_8$, are recorded. Thus, with an increase in the heat treatment time, an aluminosilicate is formed with

a lower content of strontium and with a higher content of silica.

As mentioned above, in sample no. 10, after daily heat treatment, mullite is not formed, and the sample remains a mixture of quartz and corundum, like the original charge. According to [41], $Al_2O_3$ and $SiO_2$ have a low reactivity capability, which makes direct solid-phase synthesis difficult and requires a significant increase in the firing temperature. The synthesis of single-phase mullite is associated with significant difficulties, mainly due to the low diffusion mobility of aluminum cations and silicon through the layer of mullite formed at the boundary between the particles of the original oxides. Even prolonged firing of the reaction mixture at elevated temperatures does not allow the reaction to be completed. Mullite is formed from pure silicon and aluminum oxides at a temperature of about 1873 K [42]. Since the vaporization of the $3Al_2O_3$–$2SiO_2$ system was studied at a higher temperature, the mullite was formed directly in the effusion chamber. This is indicated by the decrease in the activity of $SiO_2$ from 1 to 0.41 and the enthalpy of reaction (13) determined by us, which, within the permissible error, coincides with the reference data [43]. Determination of the temperature dependence of the $SiO^+$ ion current intensity in the mass spectrum of the vapor over sample No. 10 ($Al_6Si_2O_{13}$ mullite), made it possible to obtain the equation for the dependence of the partial pressure of SiO on temperature (17) in the temperature range 1871–2053 K and determine the enthalpy of reaction (18) at a temperature of 1995 K equal to 2108 ± 155 kJ.

$$\lg p(\mathrm{SiO},\ \mathrm{Pa}) = -\frac{27526 \pm 2046}{T} + (12.610.96), \quad (17)$$

$$Al_6Si_2O_{13}(cr) = 3Al_2O_3(cr) + 2SiO(g) + 2O(g). \quad (18)$$

The experimental data we obtained on determining the values of the activity of the components of the condensed phase indicate that the system studied by us is characterized by a negative deviation from the ideal behavior. This is due to the fact that the $SrO$–$Al_2O_3$–$SiO_2$ system is formed by oxides that differ in their acid-base properties. Strontium oxide is a typical basic oxide and forms thermally stable compounds with amphoteric aluminum oxide and acidic silica. In particular, aluminum oxide forms $Al_6Si_2O_{13}$ with silicon dioxide mullite, and in the $SrO$–$Al_2O_3$–$SiO_2$ system, according to the data of [28], there are three-component compounds: anorthite, ($SrAl_2Si_2O_8$), gehlenite ($Sr_2Al_2SiO_7$), and $Sr_6Al_{18}Si_2O_{37}$.

When strontium oxide interacts with the chamber's material, gaseous strontium tungstates can be formed [44]. The absence in the mass spectra of vapor over the studied samples of the $SrWO_3^+$ and $SrWO_3^+$, ions appears to be related to the low partial pressures of SrO and tungsten oxides.

The enthalpy of reaction (18) recalculated to a temperature of 298 K using the reference data [43] was 2143 ± 158 kJ. The value of the enthalpy of the formation of mullite from oxides at a temperature of 1995 K is –96 ± 160 kJ/mol, and at a temperature of 298 K, it is –20 ± 160 kJ/mol. The enthalpy of the formation of mullite determined in this work, of –6869 ± 160 kJ/mol, agrees well with the value of –6819.2 kJ/mol given in the reference book [43]. The obtained values of the activities of silicon and aluminum oxides for sample no. 10, which corresponds to the composition of mullite, differ from the data presented in [16, 21–23]. In our opinion, the activity of $Al_2O_3$, determined in these works, and equal to unity, does not refer to the $Al_6Si_2O_{13}$ compound, but to the region of the phase diagram of $Al_6Si_2O_{13} + Al_2O_3$. The region of the existence of mullite is quite narrow; thus, the transition from $Al_6Si_2O_{13}$ to $Al_6Si_2O_{13} + Al_2O_3$ at high temperatures occurs quite quickly due to the predominant removal of silicon oxide from the system.

## CONCLUSIONS

The processes of vaporization of the $SrO$–$Al_2O_3$–$SiO_2$ system were studied by high-temperature differential mass spectrometry at a temperature of 2000 K in the concentration range from 90 to 10 mol % SrO and the molar ratio $X(Al_2O_3)/X(SiO_2)$ of 1.5. The samples were synthesized by solid-phase synthesis from analytical grade $SrCO_3$, $Al_2O_3$, and $SiO_2$. The samples were identified by X-ray phase analysis. It has been established that an increase in the heat treatment time from 12 to 24 h at a temperature of 1523 K does not lead to a significant change in the phase composition for most samples. The melting temperatures of the synthesized samples, which lie in the range 1815–1929 K, were determined by high-temperature microscopy. It was shown that the difference in the volatility of the oxides forming the system leads to the selective evaporation of strontium and silicon oxides and the accumulation of aluminum oxide in the condensed phase. The application of the method of differential high-temperature mass spectrometry using individual oxides of strontium and silicon as standards made it possible to determine the values of the activities of SrO and $SiO_2$ at a temperature of 2000 K in the entire concentration range of compositions. For a region of a homogeneous melt, using the Gibbs–Duhem equation, the activity values of aluminum oxide were calculated and the Gibbs energies and excess Gibbs energies were determined. It is established that the studied system is characterized by the negative deviation from the ideal behavior. For mullite ($Al_6Si_2O_{13}$), the standard enthalpy of formation was determined to be –6869 ± 160 kJ/mol.

## REFERENCES


1. Chainikova, A.S., Vaganova, M.L., Shchegoleva, N.E., and Lebedeva, Yu.E., Technological aspects of the creation of radio-transparent glass-crystal materials based on high-temperature aluminosilicate systems, *Tr. VIAM,* 2015, no. 11, pp. 24–37.
2. Lisachuk, G.V., Krivobok, R.V., Zakharov, A.V., Fedorenko, E.Yu., and Trusova, Yu.D., Promising radiotransparent ceramic materials for rocket and space technology, *Vestn. NTU, Ser.: Khim., Khim. Tekhnol. Ekol.,* 2014, no. 28, pp. 72–79.
3. Shabanova, G.N., Taranenkova, V.V., Korogodskaya, A.N., and Kristich, E.V., Structure of the $BaO-Al_2O_3-SiO_2$ system (review), *Glass Ceram.,* 2003, vol. 60, nos. 1–2, pp. 43–46.
4. Lisachuk, G.V., Kryvobok, R.V., Fedorenko, E.Y., and Zakharov, A.V., Ceramic radiotransparent materials on the basis of $BaO-Al_2O_3-SiO_2$ and $SrO-Al_2O_3-SiO_2$ systems, *J. Silic. Based Compos. Mater.,* 2015, vol. 67, no. 1, pp. 20–23.
5. Kazenas, E.K. and Tsvetkov, Yu.V., *Isparenie oksidov* (Evaporation of Oxides), Moscow: Nauka, 1997.
6. Ye, X.Y., Zhuang, W.D., Wang, J.F., Yuan, W.X., and Qiao, Z.Y., Thermodynamic description of $SrO-Al_2O_3$ system and comparison with similar systems, *J. Phase Equilib. Diffus.,* 2007, vol. 28, no. 4, pp. 362–368.
7. Gantis, F., Chemekova, T.Y., and Udalov, Y.P., $SrO-Al_2O_3$ system, *Zh. Neorg. Khim.,* 1979, vol. 24, no. 2, pp. 471–475.
8. Lopatin, S.I., Shugurov, S.M., Tyurnina, N.G., Tyurnina, Z.G., and Balabanova, E.A., Vaporization and thermodynamic properties of the $SrO-Al_2O_3$ system studied by knudsen effusion mass spectrometry, *Rapid Commun. Mass Spectrom.,* 2022, vol. 36, p. e9298.
9. *Diagrammy sostoyaniya silikatnykh sistem* (Phase Diagrams of Silicate Systems), Barzakovsky, V.P., Ed., Leningrad: Nauka, 1969, vol. 1.
10. Stolyarova, V.L., Lopatin, S.I., and Tyurnina, N.G., A mass spectrometric study of evaporation processes and thermodynamic properties of $SrO-SiO_2$ melts, *Dokl. Phys. Chem.,* 2006, vol. 411, no. 1, pp. 309–311.
11. Lopatin, S.I., Shugurov, S.M., Stolyarova, V.L., and Tyurnina, N.G., Thermodynamic properties of silicate glasses and melts: II. System $SrO-SiO_2$, *Russ. J. Gen. Chem.,* 2006, vol. 76, no. 12, pp. 1878–1884.
12. Staronka, A., Pham, H., and Rolin, M., Etude du systeme silicaalumine per la methode des courbes de refroidissement, *Rev. Int. Hautes Temp. Refr.,* 1968, vol. 5, no. 2, pp. 111–115.
13. Strelkov, K.K. and Kascheev, I.D., Phase diagram of the $Al_2O_3-SiO_2$ system, *Ogneupory,* 1995, no. 8, pp. 11–14.
14. Holm, J.L. and Kleppa, O.J., Thermodynamic properties of aluminium silicates, *Am. Mineral.,* 1966, vol. 51, nos. 11–12, pp. 1608–1622.
15. Shornikov, S.I., Stolyarova, V.L., and Shultz, M.M., High temperature mass spectrometric study of $3Al_2O_3-2SiO_2$, *Rapid Commun. Mass Spectrom.,* 1994, vol. 8, no. 5, pp. 478–480.
16. Shornikov, S.I., Stolyarova, V.L., and Shul'ts, M.M., Evaporation processes and thermodynamic properties of mullite, *Dokl. Akad. Nauk,* 1994, vol. 336, no. 3, pp. 368–371.
17. Zaitsev, A.I., Litvina, A.D., and Mogutnov, B.M., Thermodynamic properties of mullite $3Al_2O_3-2SiO_2$, *Neorg. Mater.,* 1995, vol. 31, no. 6, pp. 768–772.
18. Bjorkvall, J. and Stolyarova, V.L., A mass spectrometric study of $Al_2O_3-SiO_2$ melts using a knudsen cell, *Rapid Commun. Mass Spectrom.,* 2001, vol. 15, no. 10, pp. 836–842.
19. Aksay, I.A. and Pask, J.A., Stable and metastable equilibria in the system $SiO_2-Al_2O_3$, *J. Am. Ceram. Soc.*, 1975, vol. 58, nos. 11–12, pp. 507–512.
20. Shornikov, S.I., Archakov, I.Y., and Shiltz, M.M., Vaporization processed and thermodynamic properties of the $Al_2O_3-SiO_2$ system, *Dokl. Akad. Nauk,* 1999, vol. 364, no. 5, pp. 643–646.
21. Shornikov, S.I. and Archakov, I.Yu., Vaporization processes and phase relations in the $Al_2O_3-SiO_2$ system, *Electrochem. Soc. Proc.,* 1999, vol. 99-38, pp. 339–348.
22. Shornikov, S.I., Archakov, I.Yu., and Chemekova, T.Yu., A mass spectrometric study of vaporization and phase equilibria in the $Al_2O_3-SiO_2$ system, *Zh. Fiz. Khim.,* 2000, vol. 74, no. 5, pp. 775–782.
23. Shornikov, S.I. and Archakov, I.Y., A mass spectrometric study of the thermodynamic properties of $Al_2O_3-SiO_2$ melts, *Russ. J. Phys. Chem. A,* 2000, vol. 74, no. 5, pp. 677–683.
24. Shornikov, S.I., Archakov, I.Y., and Shiltz, M.M., A mass spectrometric study of the thermodynamic properties of solid phases in the $Al_2O_3-SiO_2$ system, *Russ. J. Phys. Chem. A,* 2003, vol. 77, no. 7, pp. 1159–1166.
25. Shornikov, S.I., Archakov, I.Y., and Shiltz, M.M., A mass spectrometric study of the thermodynamic properties of mullite, *Russ. J. Phys. Chem. A,* 2003, vol. 77, no. 7, pp. 1037–1043.
26. Stolyarona, V.L., Lopatin, S.I., and Bondar', V.V., Mass-spectrometric study of system $Al_2O_3-SiO_2$, *Dokl. Akad. Nauk,* 2004, vol. 399, no. 5, pp. 644–646.
27. Bondar', V.V., Lopatin, S.I., and Stolyarona, V.L., High-temperature thermodynamic properties of the $Al_2O_3-SiO_2$ system, *Inorg. Mater.,* 2005, vol. 41, no. 4, pp. 362–369.
28. *Diagrammy sostoyaniya silikatnykh sistem* (Phase Diagrams of Silicate Systems), Toropov, N.A., Ed., Vol. 3: *Triple Systems,* Leningrad: Nauka, 1972.
29. Shukla, A., Development of a critically evaluated thermodynamic database for the systems containing alkaline-earth oxides, *PhD Thesis,* Montreal, 2012.
30. Lisachuk, G.V., Kryvobok, R.V., Zakharov, A.V., Fedorenko, E.Y., and Prytkina, M.S., Thermodynamic analysis of solid phase reactions in $SrO-Al_2O_3-SiO_2$ system, *Funct. Mater.,* 2016, vol. 23, no. 1, pp. 71–74.
31. Dear, P.S., Sub-liquidus equilibria for the ternary system $SrO-Al_2O_3-SiO_2$, *Bull. Virginia Polytech. Inst., Blacksburg,* 1957, vol. 50, no. 11, pp. 3–13; Eng. Expt. Sta. Ser. 121.
32. Starczewski, M., Treatise on solid-state reactions in the ternary system $SrO-Al_2O_3-SiO_2$, *Zesz. Nauk. Politech. Śląskiej,* 1964, vol. 22, pp. 5–75.
33. *Termodinamicheskie svoistva individual'nykh veshchestv, Spravochnik* (Thermodynamic Properties of Individual

Substances, The Handbook), Glushko, V.P., Ed., Moscow: Nauka, 1978–1982.

34. Toropov, N.A., Keler, E.K., Leonov, A.I., and Rumyantsev, P.F., High-temperature microscope, *Vestn. Akad. Nauk SSSR,* 1962, no. 3, pp. 46–48.
35. Lisachuk, G.V., Krivobok, R.V., Zakharov, A.V., Fedorenko, Ye.Yu., Prytkina, M.S., and Ryabinin, A.V., *Kosm. Tekh., Raket. Vooruzh.,* 2015, vol. 74, no. 3.
36. Sidorov, L.N. and Lopatin, S.I., High temperature chemistry applications of mass spectrometry, reference module in chemistry, molecular sciences and chemical engineering, in *Encyclopedia of Spectroscopy and Spectrometry,* 3rd ed., 2017, pp. 95–102.
37. Lias, S.G., Bartmess, J.E., Liebman, J.F., Holmes, J.L., Levin, R.D., and Mallard, W.G., Gas-phase ion and neutral thermochemistry, *J. Phys. Chem. Ref. Data,* 1988, vol. 17, no. Suppl. 1, pp. 1–861.
38. Zeifert, P.L., Measurement of vapor pressure of refractories, in *High Temperature Technology,* Kempbell, I.E., Ed., New York: Wiley, 1956, pp. 485–496.
39. Shukla, A., Development of a critically evaluated thermodynamic database for the systems containing alkaline-earth oxides, *PhD Thesis,* Montreal, 2012.
40. Morachevskii, A.G., Voronin, G.F., Geiderikh, V.A., and Kutsenok, I.B., *Elektrokhimicheskie metody issledovaniya v termodinamike metallicheskikh sistem* (Electrochemical Methods of Research in Thermodynamics of Metallic Systems), Moscow: IKTs, 2003.
41. Karagedov, G.R., Mechanochemically stimulated synthesis of single-phase mullite, *Khim. Inter. Ustoich. Razvit.,* 1998, vol. 6, pp. 161–163.
42. Balkevich, V.L., *Tekhnicheskaya keramika* (Technical Ceramics), Moscow: Stroiizdat, 1984.
43. Chase, M.W., NIST-JANAF thermochemical tables, 4th ed., *J. Phys. Chem. Ref. Data Monogr.,* 1998, vol. 9, pp. 1–1961.
44. Lopatin, S.I., Semenov, G.A., and Shugurov, S.M., Thermochemical study of gaseous salts of oxygen-containing acids: XIII. Molybdates and tungstates of alkaline-earth metals, *Russ. J. Gen. Chem.,* 2003, vol. 73, no. 2, pp. 169–175.

SPELL: 1. OK